Source:IEEE Transactions on Industrial Electronics, Vol. 59, No. 2, pp. 779-792
Year of Publication:2011
ISSN:0278-0046
Publisher:Institute of Electrical and Electronics Engineers (IEEE)
DOI:10.1109/TIE.2011.2161251

A Generalized Magnetic Circuit Modeling Approach for Design of Surface Permanent Magnet Machines

Min-Fu Hsieh, *Member, IEEE*, and You-Chiuan Hsu

***Abstract* - This paper proposes a generalized equivalent magnetic circuit model for the design of permanent-magnet (PM) electric machines. Conventional approaches have been applied to PM machine design but may be insufficiently accurate or generalized without taking pole-slot counts into consideration. This would result in reduction of dimensioning accuracy at the initial design stage. Also, magnetic saturation is often ignored or compensated by correction factors in simplified models since it is difficult to determine the flux in individual stator teeth. In this paper, the flux produced by stator winding currents and permanent magnets can be calculated accurately and rapidly using the developed model, taking saturation into account. A new modeling technique for PM poles is proposed so that the magnetic circuit is applicable to any pole-slot combinations. This aids machine dimensioning without the need for computationally expensive finite element analysis (FEA). A 540 kW PM machine is first designed using the proposed method, and then verified with FEA. Another 350 W machine is subsequently designed, manufactured and validated by both FEA and experiments. The comparisons demonstrate the effectiveness of the proposed model.**

***Index Terms*— magnetic analysis; magnetic circuit; permanent magnet machine; magnetic saturation; finite element**

LIST OF SYMBOLS

$B_{\mathrm{m,n}}$	flux density in *n-th* magnet segment
B_{new}	new flux density
B_r	remanent flux density of magnet
$C_m(n)$	effective magnet factor
$D_{n-1}\ldots D_{n+1}$	sampling points in *B-H* curve
F	absolute MMF at nodes of magnetic circuit
$F_{s,n}$	MMF in *n-th* tooth/segment
G_{fringe}	fringe permeance
$H_{\mathrm{m,n}}$	magnetic intensity of *n-th* magnet segment
H_{new}	new magnetic intensity
L_{st}	stack length (effective axial length)
N_m	number of poles
N_s	number of slots
r_{ro}	rotor radius (to magnet base)
R_l	leakage reluctance of gap between shoes
R_g	air-gap reluctance
R_m	magnet reluctance in radial direction
$R_{r,n}$	reluctance of *n-th* rotor yoke
$R_{s,n}$	reluctance of *n-th* stator yoke
$R_{t,n}$	reluctance of *n-th* tooth
r_{sl}	radius to slot outer edge
W_{open}	slot opening width
x	range of fringe permeance
μ_0	vacuum permeability
μ_{iron}	iron relative permeability
$\mu_{iron\ r,n}$	relative permeability of *n-th* rotor yoke
$\mu_{iron\ s,n}$	relative permeability of *n-th* stator yoke
$\mu_{iron\ t,n}$	relative permeability of *n-th* tooth
μ_{new}	new relative permeability
μ^*_{new}	modified permeability
μ_r	material relative permeability
θ_{eq}	effective portion of magnet in a slot pitch
θ_{mN}	angular span of N-magnet in a slot pitch
θ_{mS}	angular span of S-magnet in a slot pitch
θ_O	opening gap between two magnets
$\theta_r(n)$	remainder of relative slot angle $\theta_{sl}(n)$
θ_S	slot pitch
$\theta_{sl}(n)$	relative slot angle to a reference
$\theta_{sl}'(n)$	$\theta_{sl}(n)$ ranging between ±180°E
ϕ	flux produced from absolute MMF
$\phi_{g,n}$	flux in *n-th* air-gap
$\phi_{m,n}$	magnet remanent flux
ϕ_{new}	new flux
$\phi_{r,n}$	flux in *n-th* rotor yoke
$\phi_{s,n}$	flux in *n-th* stator yoke
$\phi_{t,n}$	flux flowing through *n-th* tooth

Manuscript received December 22, 2010; revised April 8 2011; accepted for publication November 20, 2009. This work was supported in part by the Taiwan National Science Council under Grants NSC97-2221-E-006-268-MY2, and NSC98-3114-E-006-011.

M. F. Hsieh is with the Department of Systems and Naval Mechatronic Engineering, National Cheng Kung University, Tainan 701, Taiwan (phone: +886-6-2757575 Ext. 63537; fax: +886-6-2747019; e-mail: mfhsieh@mail.ncku.edu.tw).

Y. C. Hsu is with the Department of Systems and Naval Mechatronic Engineering, National Cheng Kung University, Tainan 701, Taiwan (e-mail: f1489134@nckualumni.org.tw).

I. INTRODUCTION

Rare-earth permanent-magnet (PM) brushless machines possess the features of high efficiency, high torque/power

density and low maintenance. These advantages make them excellent candidates for various applications, such as electric vehicles [1-3], wind turbines [4-7] and marine energy converters [8].

The equivalent magnetic circuit model (EMCM) is a common technique for the analysis and design of electric machines by linking the material characteristics to the machine behavior [9-14]. The magnetic field characteristics can be technically obtained using electric circuit principles, e.g., Kirchhoff's Voltage Law (KVL) and Kirchhoff's Current Law (KCL). Magnetic saturation should also be considered as it will increase losses and degrade machine performance. Due to excessive simplifications, conventional EMCM often lacks the ability to accurately predict the flux saturation and machine performance with any pole-slot count. Correction factors based on experience may be required for compensation. Therefore, EMCM is often used for preliminary design, with confirmation or modification requiring other approaches (e.g., finite element analysis, FEA) [15]. On the other hand, some approaches may be sufficiently accurate but limited to certain pole-slot combinations.

FEA can directly calculate the flux patterns, but the entire process is computationally expensive. Changing the design parameters (dimensions, slot number, winding arrangement) in FEA often requires the model to be reconstructed. For applications where low cogging torque is advantageous (e.g., small wind turbine generators), increasing the lowest common multiple (LCM) of the PM generator is a popular solution. However, this makes it difficult to reduce the computational time by exploiting machine symmetry. Taken together, these factors account for FEA being unsuitable for the preliminary design stage of electric machines.

From the above discussion, a universal EMCM is necessary for rapid, accurate machine design of general PM machines. More delicate device models should be employed in order to improve accuracy. Modeling techniques also need to be ameliorated, e.g., a circular network that can physically represent the behavior of the flux in a machine. In particular, a reliable model for permanent magnets is a key to generalizing the model.

Tracing the history, the first related work found was offered by Roters [16] in 1941, where the analogy between the electrical and magnetic circuits was initially recognized. In [17-18], magnetic circuits were developed for analysis of self- and mutual inductances in an electrical circuit. The machine characteristics were computed via the electrical circuit but not the magnetic circuits. Carpenter [19] linked the device model of a transformer, which could be the first time the equivalent magnetic circuit was applied for analysis without an electrical circuit. Campbell [10] applied EMCM to design an axial field PM machine by assuming an infinite permeability elsewhere than the air-gap. Nady [20] built a model for PM machines with simplifications, the model of which covered one pole pitch. Vlado [21-23] conducted a series of studies to develop the EMCM for induction machines and PM machines, linking the magnetomotive forces (MMFs) of the stator winding to the main network. Nonlinear components (e.g., material saturation) were also considered. However, the main circuit was treated as a linear machine instead of circular, which could result in omission of the coupling between the first tooth and the last tooth. Gordon [24] applied the EMCM to synchronous machines, while Law *et al* [11] and Busch *et al* [25] developed an EMCM in field regulated reluctance machines, where entire machines were represented by one equivalent pole and an analogous linear machine model. Hamid *et al* [26] proposed a method for the dynamic simulation of induction machines with an analogous circular electrical network, which could, on the other hand, be complicated to calculate. Miller *et al* [27] and Hanselman [15] also contributed to EMCM, leading the approach into practical applications of PM motor design. Cheng *et al* [28] proposed a varying-network EMCM for 6/4-pole doubly salient PM motors and considered the relative position of the rotor with respect to the stator. Kano *et al* [29] improved the EMCM by developing a three dimensional network for a novel 3-D PM machine. However, the networks were complex and limited to use in PM machines with symmetric constructions. Chen *et al* [30] extended the model to a single-phase flux-switching PM motor, where the analysis was limited to two-pole or symmetric structures. Han *et al* [31] also reported work on magnetic circuit for PM motors. To sum up, the above mentioned literature rarely considered the detailed model for permanent magnet poles - contribution of North and South pole magnets to the flux in each tooth (and so the flux linkage) for any relative rotor position to the stator. This implies that they may not be sufficiently generalized for any pole-slot combinations.

In this paper, a generalized, accurate and time-effective EMCM for design and analysis of surface PM machines is proposed, taking pole-slot count and flux saturation into account. The model employs a circular configuration that covers all the magnetic loops on all the stator teeth to enhance the accuracy. This ensures that the flux patterns of machines with any pole-slot counts and winding can be calculated. In this model, the MMFs produced by the windings are computed to determine the material permeability (operating point) according to the *B-H* curve so that the flux can be accurately obtained. This calculation is performed simultaneously for all the MMF sources, including the rotor magnets. The MMF sources of the magnets are treated in a piecewise fashion, i.e. the magnets are virtually modularized into several segments to associate with stator slots for fitting into the magnetic network. This segmented PM model (detailed later) is a major contribution of this paper. This allows the proposed EMCM to be applicable to any pole-slot combinations and to be more generalized than conventional approaches. Consequently, the flux in different locations of the machines can be accurately calculated and the locations where magnetic saturation occurs can also be predicted. By integrating the above features, this solution can thus provide rapid and accurate machine design. Simulation of a 540 kW machine and experiments on a 350W machine are used to verify the developed model.

II. Machine Modeling

A. Loading on Magnetic Circuits

In the EMCM, the accuracy of the model depends on the accuracy of individual component models and the coupling between the active components (e.g., magnet and winding) and passive components (e.g., air gap and iron core). This requires a careful study on loadings of the magnetic circuits. In common operation of a PM machine, the magnetic loading and electric loading are simultaneously applied. The magnetic circuit can accommodate flux to a certain level regardless of the magnetic sources, but this ability depends on the material characteristics and geometry. Generally, for a proper design, the magnetic circuit should accommodate more flux than an inappropriate one to achieve the required specifications. The operating points of ferromagnetic materials (nonlinear), associated with the magnetic loading conditions, should be as close to the peak permeability on the μ-H curve as possible. This indicates that the magnetic loading should be designed around that level to maximize the flux accommodation via the most economic magnetic intensity without saturating the materials. Care should be taken in the analysis to achieve this economic design considering both the material and geometry.

The sensitivity of nonlinear materials is studied here to help refine the highly sensitive components in the EMCM so that the design accuracy in the initial stage can be improved. A simple C-type magnetic circuit, shown in Fig. 1, is used for this study, the parameters of which are detailed in Table I.

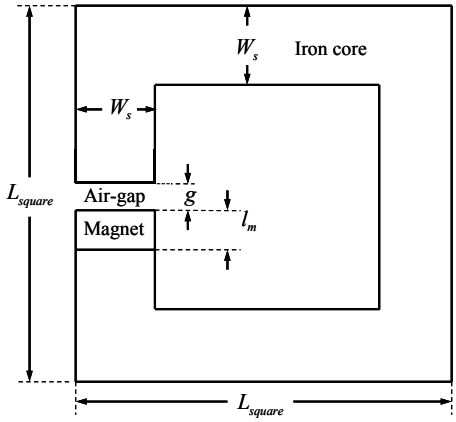

Fig. 1 Definitions of parameters in a C-type circuit

Material with high permeability is expected to operate at high flux density. Here, an iterative process is used to calculate the correct permeability for the C-type circuit under a magnetic field according to the material's B-H and μ-H curves for improving the accuracy.

TABLE I
SIMULATION PARAMETERS FOR C-TYPE MODEL

Parameter/Symbol		Value	Unit
Magnet length (l_m)		5	mm
Tooth width (W_s)		20	mm
Air-gap length (g)		1.0	mm
Case length (L_{square})		100	mm
Magnet	Remanent flux density (B_r)	1.23	T
	Coercive force (H_c)	930	kA/m
	Relative permeability (μ_r)	1.05	--

FEA simulation (ANSOFT Maxwell) is employed for the flux calculation of the C core. Typical iron core material usually has relative peak permeability between 4000 and 8000 [15], [32]. The flux at a relative permeability of the mean value (=6000) is therefore used to normalize the flux under different material permeability, as shown in Figs. 2(a) and (b). In Fig. 2(b), the percentage difference for the normalized flux (based on μ_r=6000) between μ_r=4000 and 8000 is 1.2% (-0.88% for μ_r =4000 and 0.32% for μ_r =8000). Despite being well known, it is here concluded that in high permeability operations, the error produced from incorrect permeability can be ignored, while a nonlinear material can be treated as linear with its maximum permeability.

B. Modeling of Permanent Magnets

This section discusses the modeling of permanent magnets in a PM machine by considering stator slots/teeth and rotor position. As previously mentioned, this PM model enables the proposed EMCM to analyze and design machines with any pole-slot combinations. Flux leakage occurs when the flux produced by a magnet fails to flow through the stator windings and thus contributes no magnitude to the back-EMF. The level of flux leakage depends on the pole-to-slot ratio, slot geometric features, and rotor position. Three conditions are considered here. First, the "flux cancellation" mode accounts for the most serious flux leakage, as shown in Fig. 3(a). Second, in the "partial contribution" mode, part of one pole is within a slot pitch. The contribution of flux from the magnet is mitigated due to the gap between the two magnets (magnet opening), as shown in Fig. 3(b). Third, for the "full contribution" mode in Fig. 3(c), the whole slot pitch is covered by one pole, where all the flux produced by the magnet is treated as flowing through the tooth.

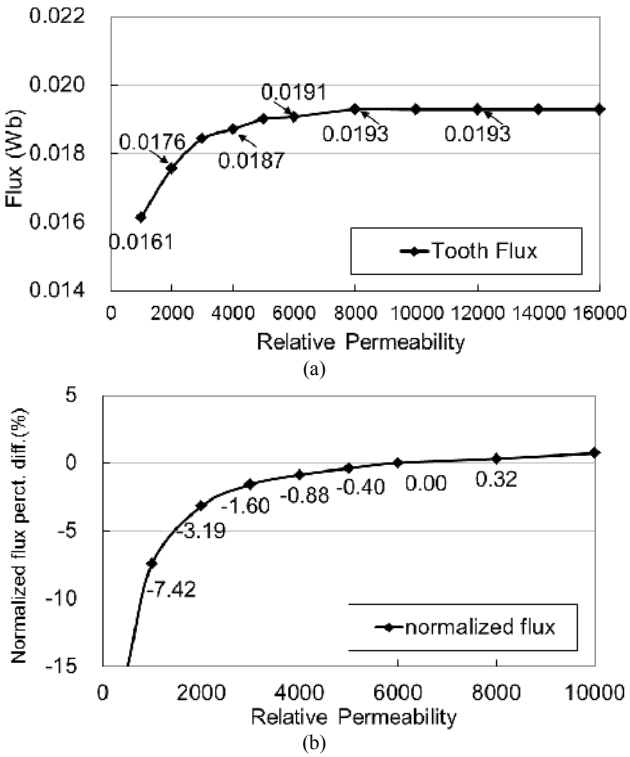

Fig. 2 C-type circuit (with 1mm air-gap): (a) flux and (b) percentage difference of normalized flux based on μ_r=6000.

Based on the previous analysis, the PM model is derived. Considering a slot pitch θ_S, it is assumed that the contribution of the magnet to MMF is proportional to the portion of the magnet within θ_S, as indicated in Fig. 4. For the slot pitch of the *n-th* tooth (or segment), the opening gap between the two magnets is denoted by θ_O, the angle for the N-pole magnet is represented by θ_{mN}, while θ_{mS} denotes that of the S-pole magnet.

The effective portion of the magnet (denoted as angle θ_{eq}) in a slot pitch can be expressed as

$$\theta_{eq} = C_m \cdot \theta_S \tag{1}$$

where C_m is defined as the *effective magnet factor* for a tooth/segment and can be defined as

$$C_m = \frac{\theta_{mN} - \theta_{mS}}{\theta_S}, \quad -1 \le C_m \le 1 \tag{2}$$

It should be noted that C_m varies with tooth sequence and hence the relative rotor-stator position. For example, C_m=1 (tooth facing North pole) and C_m= -1 (tooth facing South pole) represent the "full contribution modes", as shown in Fig. 3(c). Likewise, C_m=0 is in the flux "cancellation model" while other values in the "partial contribution mode." Therefore, it is necessary to calculate C_m for every single tooth or segment no matter what pole-slot combinations is so that the coil flux linkage can be determined. C_m can therefore be written as a function of *n-th* tooth as follows:

$$C_m = C_m(n) \tag{3}$$

where n represents the tooth or segment sequence. By (1) - (3), this method can cover machines with any pole-slot combinations. The value of C_m can be obtained by the following process and parameters.

Step1 – calculation of slot pitch

The slot pitch in electrical degrees can be written as:

$$\theta_S = \frac{360}{N_s} \cdot \frac{N_m}{2} \tag{4}$$

where N_m is the number of poles and N_s is the number of slots.

Step2 – calculation of relative tooth angle

The relative slot angle θ_{sl} (n) to a reference for the *n-th* tooth/segment in electrical degrees is defined as a function of tooth/segment sequence n.

$$\theta_{sl}(n) = (n-1) \cdot \theta_S, \; n = 1, 2, 3 \ldots N_s \tag{5}$$

For simplification, only the remainder of θ_{sl} (n) divided by an electrical period of 360° is needed, which can be expressed as

$$\theta_r(n) = \mathrm{Rem}\left\{\theta_{sl}(n),\ 360^o\right\} \tag{6}$$

Step3 – magnet polarity associated with tooth/segment

The sign of $\theta_r(n)$ in (6) is used to recognize the polarity of the magnet. The N-pole magnet is defined as positive; while the S-pole magnet negative.

$$Sign\left(\theta_r(n)\right) = \begin{cases} 1, & \theta_r(n) \le 180^o \\ -1, & otherwise \end{cases} \tag{7}$$

Step4 – rearrangement of relative tooth angle

Because $\theta_{sl}(n)$ has a period of 360°E, it can be treated within the range of ±180°E, as given below:

$$\theta_{sl}'(n) = \mathrm{Rem}\left\{\theta_{sl}(n) + 180^o,\ 360^o\right\} - 180^o \tag{8}$$

In order to facilitate the interpretation, $\theta_{sl}'(n)$ can be observed on the *polar-coordinate plane*. As shown in Fig. 5, it is found that $\theta_{sl}'(n)$ is reciprocal in the first- and third-quadrant (and also in the second- and fourth-quadrant). Therefore, an arbitrary additive of ±180°E does not result in any change in the calculation of C_m.

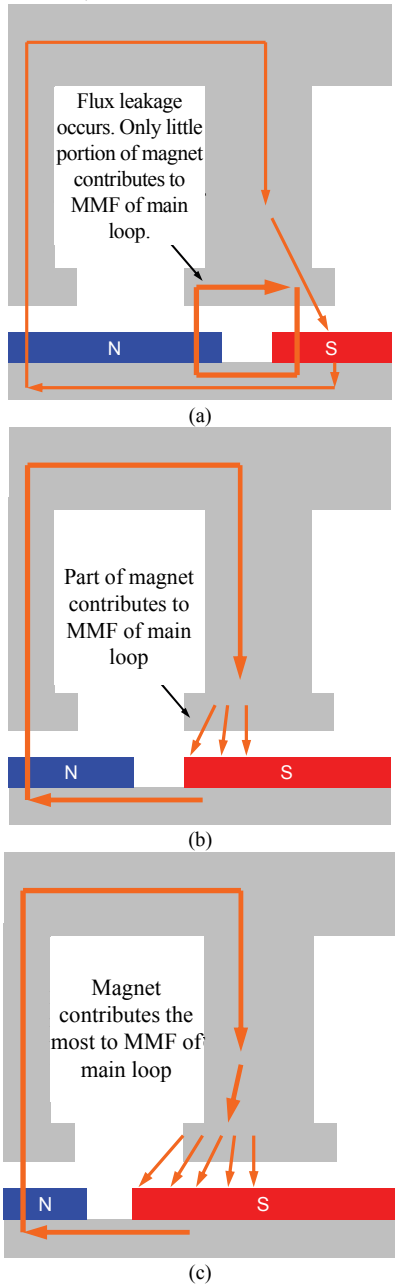

Fig. 3 Flux distributions varying with the rotor position: (a) flux cancellation, (b) partial contribution and (c) full contribution

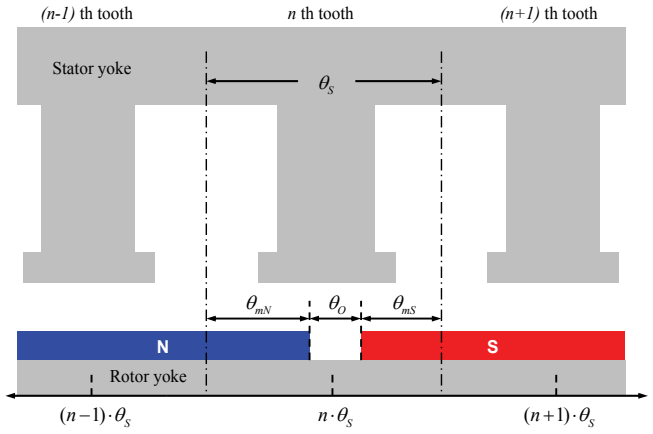

Fig. 4 Features of magnet within a slot pitch

In Fig. 5, the imaginary axis demonstrates the polarity of the magnet-piece within a slot pitch. The status of C_m can be obtained by observing the projection on the real axis. Moreover, the $\theta_{sl}'(n)$ can be further treated within the ±90°E range for convenience.

$$\theta_{sl}'(n)=\begin{cases}\theta_{sl}'(n)-180^o, & \theta_{sl}'(n)\ge 180^o\\ \theta_{sl}'(n)+180^o, & \theta_{sl}'(n)\le -180^o\end{cases} \tag{9}$$

As shown in Figs. 5 and 6, the two boundaries, *a* and *b*, of the flux partial contribution modes are given as:

$$a=\mathrm{Re}\left\{e^{j\left(\frac{\theta_S-\theta_O}{2}\right)}\right\} \tag{10}$$

$$b=\mathrm{Re}\left\{e^{j\left(\frac{\theta_S+\theta_O}{2}\right)}\right\} \tag{11}$$

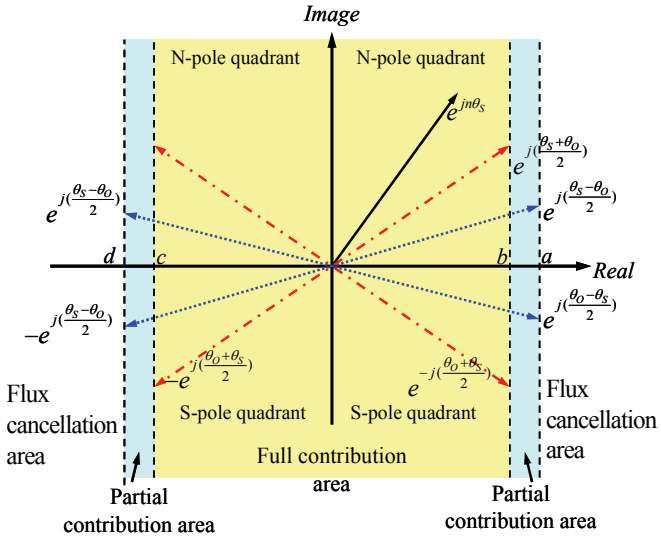

Fig. 5 The modified slot angle $\theta_{sl}'(n)$ in polar-coordinate plane

Step5 – Determination of $C_m(n)$

Finally, $C_m(n)$ varying with the tooth sequence and rotor position can be expressed as

$$C_m(n)=\begin{cases}Sign\left(\theta_r(n)\right), & \mathrm{Re}\left\{e^{j\cdot\theta_{sl}'(n)}\right\}\le b\\ Sign\left(\theta_r(n)\right)\cdot\left[1-\dfrac{\frac{\theta_S-\theta_O}{2}-\left|\theta_{sl}'(n)\right|}{\theta_S}\right], & b<\mathrm{Re}\left\{e^{j\cdot\theta_{sl}'(n)}\right\}<a\\ Sign\left(\theta_r(n)\right)\cdot\dfrac{2\left|\theta_{sl}'(n)\right|}{\theta_S}, & \mathrm{Re}\left\{e^{j\cdot\theta_{sl}'(n)}\right\}\ge a\end{cases} \tag{12}$$

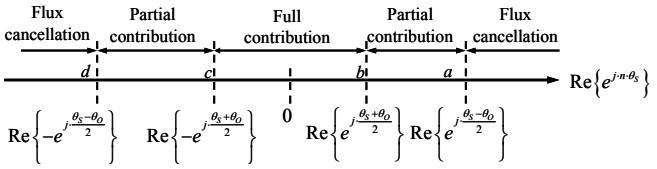

Fig. 6 Boundaries of the modes on the real-axis

C. *Modeling of General PM Machines*

The above rotor PM model is incorporated into the developed EMCM for the design of PM electric machines. The flux produced by the stator winding currents and rotor PMs are calculated for each stator tooth, taking saturation into account. The permeability is updated according to the calculation result of the previous round in an iterative process. A circular network is established for the PM machines, where the flux loop and nodal equations (i.e. KCL and KVL) are employed to solve the complex issues.

1) *Permeance matrix*

All of the components in the magnetic circuit are modeled in accordance with the machine's geometric configuration and material characteristics. The definitions of the parameters, given in Fig. 7, are based on the geometry of a slot for general PM machines. Other related parameters include the vacuum permeability μ_0, stack length (effective axial length) L_{st}, number of slots N_s and iron relative permeability μ_{iron}.

Assumptions are made prior to the development of the proposed model:

(a) The permeability of the iron core is variable, as expressed using the variable reluctances shown in Fig. 8. They are all individually considered.

(b) The flux flowing through one stator tooth flows through the air gap uniformly within a slot pitch.

(c) The rotor is slotless.

As demonstrated in Figs. 7 and 8, the air-gap reluctance R_g is defined as:

$$R_g=\frac{N_s\cdot g}{2\pi\cdot\mu_0\cdot(r_{ro}+l_m+0.5\cdot g)\cdot L_{st}} \tag{13}$$

The reluctance of the *n-th* tooth $R_{t,n}$, the *n-th* rotor yoke $R_{r,n}$, and the *n-th* stator yoke $R_{s,n}$ (stator and rotor yoke segmented into the number of slots) are respectively expressed as

$$R_{t,n}(\mu_{iron\_t,n})=\frac{(r_{sl}-g-r_{ro}-l_m+0.5\cdot W_{yoke\_s})}{\mu_{iron\_t,n}\cdot\mu_0\cdot W_t\cdot L_{st}} \tag{14}$$

$$R_{r,n}(\mu_{iron\_r,n}) = \frac{\pi \cdot (2r_{ro} - W_{yoke\_r})}{N_s \cdot \mu_{iron\_r,n} \cdot \mu_0 \cdot W_{yoke\_r} \cdot L_{st}} + \frac{W_{yoke\_r} \cdot N_s}{\pi \cdot \mu_{iron\_r,n} \cdot \mu_0 \cdot (r_{ro} - 0.25W_{yoke\_r}) \cdot L_{st}} \quad (15)$$

$$R_{s,n}(\mu_{iron\_s,n}) = \frac{\pi \cdot (2r_{sl} + W_{yoke\_s})}{N_s \cdot \mu_{iron\_s,n} \cdot \mu_0 \cdot W_{yoke\_s} \cdot L_{st}} \quad (16)$$

where $\mu_{iron\_t,n}$ is the relative permeability of the *n-th* tooth, $\mu_{iron\_r,n}$ is that of the *n-th* rotor yoke, and $\mu_{iron\_s,n}$ is that of the *n-th* stator yoke. These parameters may alter during the iteration process and this will be detailed later. The reluctance of the magnet in the radial direction is

$$R_m = \frac{N_s \cdot l_m}{2\pi \cdot \mu_m \cdot \mu_0 \cdot (r_{ro} + 0.5 \cdot l_m) \cdot L_{st}} \quad (17)$$

It should be noted that the magnet remanent flux $\phi_{m,n}$ and other undefined symbols so far will be addressed later.

The flux leakage between two shoes on two adjacent shoes is considered. As can be seen in Fig. 9, the slot opening permeance between the two shoes (slot opening width W_{open}) is subject to the fringing effect so that modification with a correction factor is needed to enhance the modeling accuracy.

For the flux pattern in one side of the shoe, as shown in Fig. 9, the fringe permeance model of a lateral flat with the associated parameters can be expressed as [15, 33]

$$G_{fringe} = \mu_0 \cdot \frac{x \cdot H_{shoe}}{0.17 \cdot W_{open} + 0.4 \cdot x} \quad (18)$$

where x is the range to which the fringing permeance extends. The range x is not fixed by any other geometric constraint and the exact value chosen is not critical since the contribution of differential permeances decreases as x increases. The gap length is W_{open} in this case. Based on (18), the complete *leakage reluctance of the shoe gap* R_l, taking into account all four sides, can be modeled as

$$R_l = \left[\frac{0.17 \cdot W_{open} + 0.4 \cdot x}{2 \cdot \mu_0 \cdot x \cdot (H_{shoe} + L_{st})} + \frac{W_{open}}{\mu_0 \cdot H_{shoe} \cdot L_{st}} \right]^{-1} \quad (19)$$

It should be noted that the leakage flux between the two adjacent shoes travels through the air (Fig. 9) so that it is not related to the shoe material permeability. It is known that the shoes can be easily saturated and present a nonlinear behavior, but the effect on the overall machine performance is minor and hence neglected here.

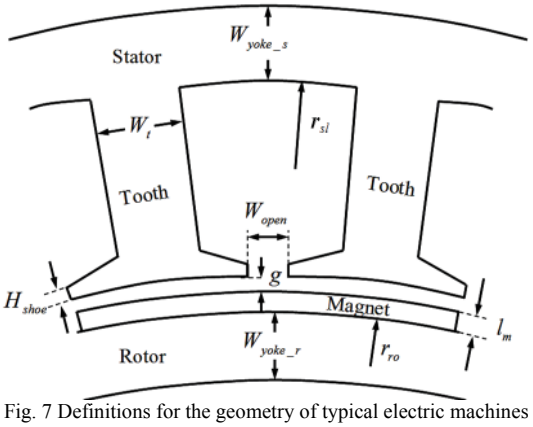

Fig. 7 Definitions for the geometry of typical electric machines

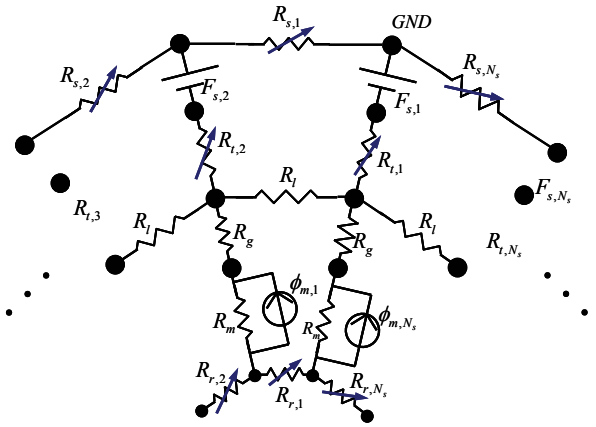

Fig. 8 Machine modeling: definitions for magnetic components. A full-size node-definition-map of the 24-slot PM machine is established but not demonstrated here for brevity.

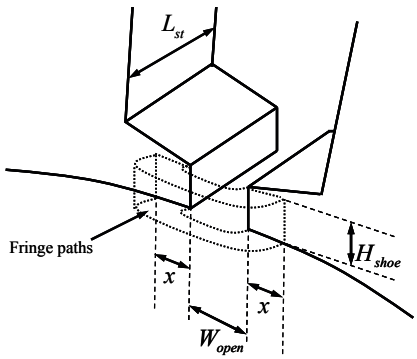

Fig. 9 Configuration of a shoe: flux pattern between shoes (one side shown)

The ampere-turns in one slot is represented by an MMF source. All these magnetic components used in the magnetic network are shown in Fig. 8, where $F_{s,n}$ represents the MMF in the *n-th* tooth/segment. Note that the reluctances in (14)-(16) are numbered (e.g., $R_{s,1}$ to $R_{s,Ns}$) by the segments shown in Fig. 8, while the definitions of the nodes are given in Fig. 10.

Any N_s slot machine can be modeled and the corresponding EMCM can be constructed once N_s is determined. In this study, the EMCM is expressed using a matrix which can be solved by KCL/KVL with the aid of computer programming. The details of the model are given in the following derivation. First, all of the parameters based on the machine geometry, materials, and winding layouts, as discussed above, are arranged in a matrix of size $(6N_s\text{-}1)\times(6N_s\text{-}1)$, defined as "Permeance Matrix A" (the size of the matrix is a function of N_s), given as:

$$A = \begin{bmatrix} G & B \\ C & D \end{bmatrix}_{(6N_s-1)\times(6N_s-1)} \quad (20)$$

where G is a $(5N_s\text{-}1)\times(5N_s\text{-}1)$ matrix and function of N_s consisting of sixteen sub-matrices (Matrices B, C and D will be explained later).

Matrix G is arranged as follows:

$$G(N_s) = \begin{bmatrix} G_1 & G_2 & G_3 & G_4 & G_5 \\ G_6 & G_7 & G_8 & G_9 & G_{10} \\ G_{11} & G_{12} & G_{13} & G_{14} & G_{15} \\ G_{16} & G_{17} & G_{18} & G_{19} & G_{20} \\ G_{21} & G_{22} & G_{23} & G_{24} & G_{25} \end{bmatrix}_{(5N_s-1)\times(5N_s-1)} \quad (21)$$

The details of the sub-matrices (G_1–G_{25}) contained in Matrix G are given in the appendix (equations A.1-A.21), where all the parameters can be obtained from (13) to (19). It is noted that these matrices have different sizes, and the combination of them will form the Matrix G.

Matrix B in (20) is in the form of Boolean functions whose signs are determined by the direction of the MMF sources due to winding currents. Generally, Matrix B can be expressed by the following equations:

$$B = \begin{bmatrix} B_1 \\ B_2 \\ B_3 \end{bmatrix}_{(5N_s-1)\times N_s} \tag{22}$$

where

$$B_1 = diag\left[1\right]_{N_s\times N_s} \tag{23}$$

$$B_2 = \begin{bmatrix} 0 & -1 & \cdots & 0 \\ \vdots & & \ddots & \vdots \\ & & & 0 \\ 0 & \cdots & & -1 \end{bmatrix}_{(N_s-1)\times N_s} \tag{24}$$

$$B_3 = [0]_{3N_s\times N_s} \tag{25}$$

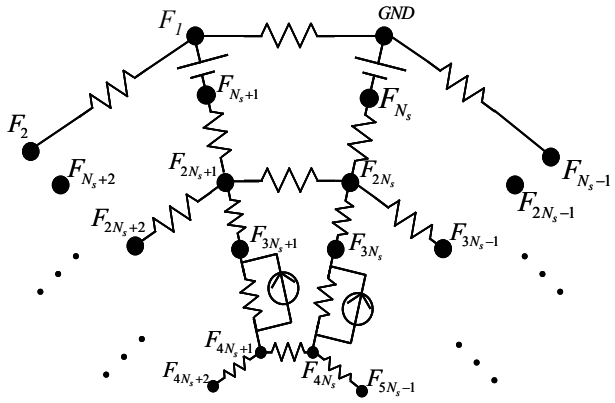

Fig. 10 Machine modeling: definitions for the nodes

Matrix C is a transpose matrix of B, while D is a zero matrix.

$$C = B^T \tag{26}$$

$$D = \left[0\right]_{N_s\times N_s} \tag{27}$$

To construct the model, the relationship between MMF sources and flux produced needs to be determined. Matrix $\overline{x}$ is hence introduced, which is given as:

$$\overline{x} = \begin{bmatrix} F \\ \phi \end{bmatrix}_{(6N_s-1)\times 1} \tag{28}$$

where F indicates the absolute MMF at the nodes of the network as defined in Fig. 10, and ϕ represents the flux produced from F. F and ϕ are respectively given by:

$$F = \left[F_1 \quad F_2 \quad \cdots \quad F_{5Ns-1}\right]^T_{(5Ns-1)\times 1} \tag{29}$$

$$\phi = \left[\phi_1 \quad \phi_2 \quad \cdots \quad \phi_{N_s}\right]^T_{N_s\times 1} \tag{30}$$

The elements in matrix ϕ represents the assembly of the fluxes associated with the *n-th* tooth/segment, such as the tooth flux, air-gap flux, stator yoke flux and rotor yoke flux. These will be detailed later. The magnitude of the external MMF produced from the winding current and the magnets can be defined by a matrix z:

$$z = \left[Z_1 \quad Z_2 \quad Z_3 \quad Z_4\right]^T_{(6Ns-1)\times 1} \tag{31}$$

where

$$Z_1 = \left[0\right]_{(3Ns-1)\times 1} \tag{32}$$

$$Z_2 = -Z_3 = \left[\phi_{m,1} \quad \phi_{m,2} \quad \cdots \quad \phi_{m,N_s}\right]^T_{Ns} \tag{33}$$

and where $\phi_{m,1}$ … $\phi_{m,Ns}$ are the flux sources produced from the *n-th* segment of the magnets (addressed in the previous section). The equivalent flux source produced from the permanent magnets for the *n-th* tooth/segment can then be expressed as

$$\phi_{m,n} = B_r \cdot \tau_{mag} \cdot C_m(n) \cdot \frac{2\pi \cdot \left(r_{ro} + 0.5 \cdot l_m\right) \cdot L_{st}}{N_s} \tag{34}$$

where $0 \leqq \tau_{mag} \leqq 1$, representing, in a pole pitch, the ratio of actual magnet to the pole pitch. This takes out of account the gaps between the magnet poles containing no magnet since they do not produce flux. When C_m=1 or -1 for a certain tooth/segment, the magnet within that segment becomes a fully dedicated source.

The MMF source $F_{s,n}$ produced from the winding current in the *n-th* slot can be expressed as Z_4, which is

$$Z_4 = \left[F_{s,1} \quad F_{s,2} \quad \cdots \quad F_{s,N_s}\right]^T_{Ns} \tag{35}$$

It should be noted that the $F_{s,n}$ here (the MMF sources determined from the winding currents) and the F (absolute MMF at the nodes) in (29) are different. Finally, matrix $\overline{x}$ can be obtained using the following equation.

$$\overline{x} = A^{-1} z \tag{36}$$

where A^{-1} is the inverse of Matrix A in (20). To determine the material operating points, the flux in various components of the machine is calculated. The flux flowing through the n-th tooth, $\phi_{t,n}$, can be expressed as

$$\begin{cases} \phi_{t,n} = \dfrac{F_{n+N_s} - F_{n+2N_s}}{R_{t,n}}, & n = 1, 2, \cdots, N_s - 1 \\ \phi_{t,N_s} = \dfrac{-F_{2N_s}}{R_{t,n}}, & n = N_s \end{cases} \tag{37}$$

The flux in the *n-th* air-gap, $\phi_{g,n}$, can be given by

$$\phi_{g,n} = \frac{F_{2N_s+n-1} - F_{n+3N_s-1}}{R_g}, \quad n = 1, 2, \cdots, N_s \tag{38}$$

Again, the flux in the *n-th* stator yoke, $\phi_{s,n}$, is

$$\begin{cases} \phi_{s,n} = \dfrac{F_n - F_{n+N}}{R_{s,n}}, & n = 1,2,\cdots,N_s - 1 \\ \phi_{s,n} = \dfrac{F_{N_s}}{R_{s,n}}, & n = N_s \end{cases} \tag{39}$$

For the flux in the *n-th* rotor yoke $\phi_{r,n}$

$$\begin{cases} \phi_{r,n} = \dfrac{F_{4N_s+n} - F_{n+4N_s+1}}{R_{r,n}}, & n = 1,2,\cdots,N_s - 1 \\ \phi_{r,n} = \dfrac{F_{5N_s-1} - F_{4N_s}}{R_{r,n}}, & n = N_s \end{cases} \tag{40}$$

For the magnets, the flux density in the *n-th* segment of magnet $B_{\mathrm{m,n}}$ is given by

$$B_{m,n} = \frac{N_s \cdot \left(F_{3N_s+n-1} - F_{n+4N_s-1}\right)}{2\pi \cdot r_{ro} \cdot L_{st} \cdot R_m}, \quad n = 1,2,\cdots,N_s \tag{41}$$

The magnetic intensity in the *n*-th segment of magnet $H_{\mathrm{m,n}}$ is

$$H_{m,n} = \frac{F_{3N_s+n-1} - F_{n+4N_s-1}}{l_m}, \quad n = 1,2,\cdots,N_s \tag{42}$$

In the proposed EMCM, the networks are treated as a function of N_s; therefore, the approach can be easily extended to general machines with any number of slots and poles. There is no need to rebuild the network for each particular case. This approach can also be expanded to other electric machines with an appropriate modification.

D. Nonlinear Material Considerations

For nonlinear materials, the permeability varies with operating points. Therefore, the permeability of the primary components in the EMCM (i.e. the teeth (14), rotor yokes (15), and stator yokes (16)) needs to be updated frequently by an iterative process.

1) Iterative process of the EMCM

An arbitrary but reasonable permeability of 4000 is initially given to the nonlinear materials in the EMCM to initiate the calculation, as shown in (14)-(16). After the first round of calculation, a new condition for the EMCM can be observed and the new flux ϕ_{new} in the primary components can be derived by (38) and (40)-(41). The new flux density B_{new} can consequently be calculated using

$$B_{new} = \frac{\phi_{new}}{A} \tag{43}$$

where ϕ_{new} represents the flux and A is a cross-section where ϕ_{new} passes through. The B_{new} of the component acquires a new magnetic intensity H_{new} from the operating points on the *B-H* profile. The new relative permeability of the component becomes

$$\mu_{new} = \frac{\Delta B_{new}}{\Delta H_{new}} \tag{44}$$

Finally, the μ_{new} is fed back to the EMCM to replace the initial value of the component, thus completing one round of the iteration. More iteration is usually needed to help the process converge. The approach to obtain H_{new} from the *B-H* profile and to update permeability is addressed below.

2) Permeability update for the nonlinear materials

A piecewise method is used to describe the *B-H* profile of the nonlinear material for the saturation effect since the measured points provided by manufacturers are limited. In this paper, an internal-insertion method is employed to obtain the new permeability in each iteration process. Consider the condition where B_{new} is located between two consecutive sampling points (D_n and D_{n+1}) of the nonlinear material hysteresis loop, as shown in Fig. 11. If the sampling rate of the data is sufficient, the curve between D_n and D_{n+1} can be treated as a straight line. The H_{new} can therefore be comprehensively written as

$$H_{new} = H_n + \left(H_{n+1} - H_n\right) \cdot \frac{B_{new} - B_n}{B_{n+1} - B_n} \tag{45}$$

In order to prevent divergence and increase the stability of the iterating process, the replacement approach (45) is improved using a reference to the last value of the component. For instance, before feeding μ_{new} back to replace the previous value, an average of μ_{new} and previous value μ_{old} is taken.

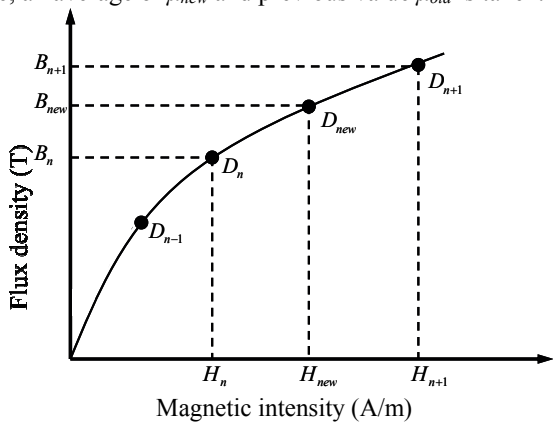

Fig. 11 *B-H* curve of nonlinear materials

The modified permeability μ^*_{new} can be expressed as

$$\mu^*_{new} = \frac{\mu_{new} + \mu_{old}}{2} \tag{46}$$

To summarize the iterative process, this approach for a particular rotor position is detailed in Fig. 12.

III. FEA AND EXPERIMENTAL VERIFICATIONS

Two machines were used for demonstration. The first machine is a 540 kW 40-pole 60-slot machine designed with the proposed EMCM. This 540 kW PM machine was designed for a wind turbine generator (non-direct drive). For such an application, large air gap may be required. Hence, the air gap is modified to two times the original design. For these two air gaps, the EMCM was compared with FEA for both the open circuit and loaded conditions.

The other machine is a 350W 16-pole 24-slot machine, which was verified by both FEA and experiments. In this machine, a given stator core was used for convenience, and other parts (i.e., the stator windings and rotor) were designed and constructed using the proposed method.

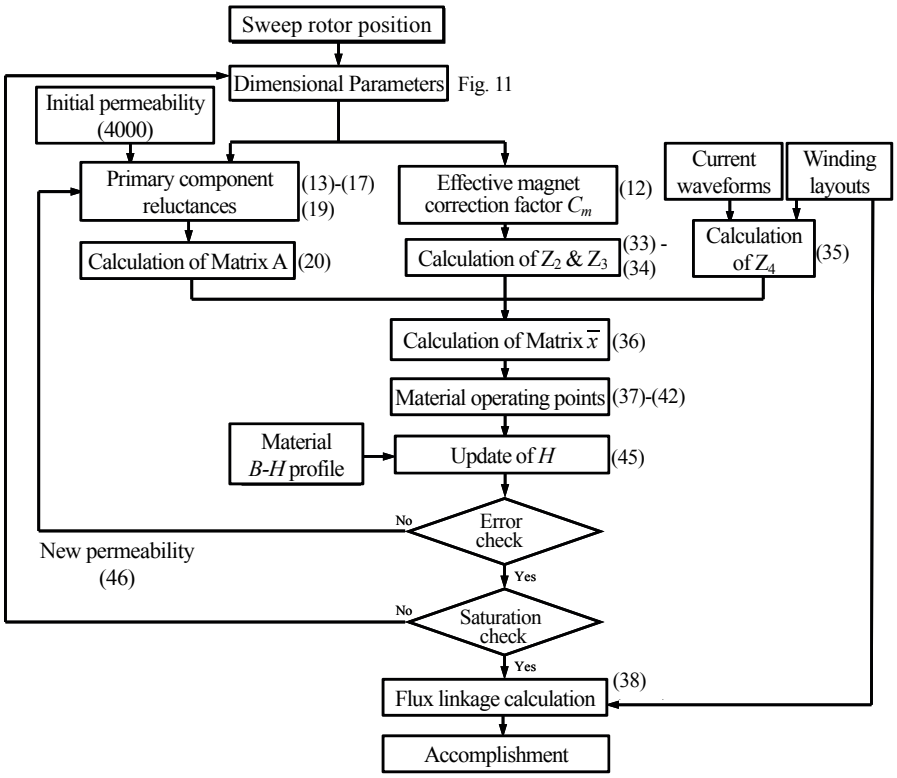

Fig. 12 Iterating process of the EMCM approach

TABLE II
SPECIFICATIONS OF 540 KW MACHINE

Operating speed (r.p.m.)	610
Output power (kW)	540
Generator efficiency (%)	90
Generator input power (kW)	600
Required output torque (kN-m)	9.39
Current density (A_{rms}/mm^2)	8
Rated current (A_{rms})	451.8
Slot filled ratio (%)	35
Open-Circuit phase voltage (V_{rms})	442.7
Rated/loaded phase voltage (V_{rms})	398.4
Line-to-line voltage (V_{rms})	690
Phase back-EMF constant $\|K_e\|$ (V.s/radM)	9.8

TABLE III
DESIGN RESULTS OF 540 KW MACHINE

Pole number		40	Copper area (mm^2)	56.5
Slot number		60	Copper diameter (mm)	5.2
Number of turns per coil		3	Tooth width (mm)	20
Parallel paths		2	Tooth height (mm)	108
Air-gap flux density (T)		0.96	Rotor yoke width (mm)	26.6
Air-gap (mm)		1.5	Stator yoke width (mm)	28
Magnet length (mm)		6.9	Stack length (m)	0.315
Magnet (*NdFeB*)	B_r (T)	1.19	Rotor radius r_{ro} (mm)	291.6
	H_{cb} (kA/m)	883	r_{sl} (mm)	417
	H_{cj} (kA/m)	≧1353	Stator outer rad. (mm)	445
Slot opening (mm)		10	Stator inner rad. (mm)	300
Slot area (mm^2)		968	Shoe height (mm)	3

A. 540 kW Machine with FEA Verification

1) Original design

The specifications for the prospective 540 kW generator are detailed in Table II. The generator is expected to offer a phase voltage of 398.4 V_{rms} at 610 rpm. The design results and material characteristics are detailed in Table III, while the sample FEA model is presented in Fig. 13. The winding design in this study follows the approach in [15], which is well known and not detailed here. A 10% pole pitch is used to gap the two adjacent magnets, mitigating the flux leakage effect. The 10% pole pitch in this case is equivalent to 0.9°M, which can be used to calculate C_m in (12). The *B-H* profile of the 50CSC1300 soft iron [32] is created in MATLAB using an iterative process. The back-EMF constant waveform is obtained using the derivation of the flux linkages, which is collected from the flux within the teeth. Equation (38) is used to calculate the flux linkage with respect to the winding.

The comparison between the developed EMCM and FEA is shown in Fig. 14(a) and (b), where the former is without magnet skew and the latter is with skew. These skewed results are simply calculated by superimposing them with the original (as shown in Fig. 14(a)) and shifting (shift 1.5°M of the waveforms in Fig. 14(b)) the waveforms. As can be seen, the back-EMF constant generated from these two approaches both match the specifications.

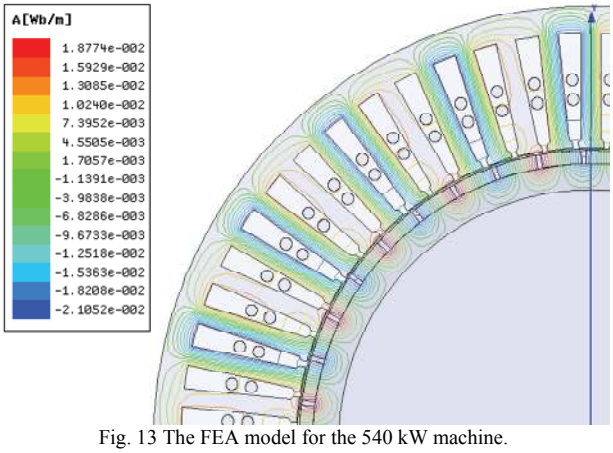

Fig. 13 The FEA model for the 540 kW machine.

2) Design with larger air gap

The large air-gap design has a magnet length of 13.8 mm to maintain the magnet operating point. All the rest parameters remain the same. As can be seen in Fig. 15, the back-EMF constants are very similar for the case with g=1.5 mm (the ratio of air-gap length to magnetic pole arc is around 1/28) and that with g=3 mm (the ratio of air-gap length to magnetic pole arc is around 1/14). For g=3 mm, the proposed EMCM also has a close waveform to the FEA. This accounts for the effectiveness of the proposed method in dealing with large air gaps.

3) Simulation under rated load

The machine (for both g=1.5 mm and g=3 mm) is loaded with the rated current. The comparison of flux density between the FEA and the proposed EMCM is shown in Table IV, where the maximum flux density on teeth is calculated for open-circuit and loaded conditions. As can be seen, for all the cases, the EMCM matches FEA very well. The operating point of the tooth magnetic material has been well above the knee area of the *B-H* curve under rated load, and this indicates some saturation. Fig. 16 shows the iterative calculations for tooth operating points when the machine (g=1.5 mm) is loaded using the developed EMCM and computer program. The dots on the *B-H* curve represent the operating points, and the final point (calculation completed) has a flux density of 1.7 T, as indicated in Table IV. Therefore, the proposed EMCM is capable of reflecting the saturation effect when the machine is loaded. It should be noted that the FEA simulations for the loaded case give a torque of 9.28 kN-m and 9.20 kN-m for g=1.5 mm and g=3 mm, respectively (designed rated torque=9.39 kN-m). This verifies that the machine can be loaded to the rated point.

B. 350 W Machine with FEA and Experiments

As demonstrated in Fig. 17(a) and (b), a skew angle of 3.75°M is employed in this study to reduce the cogging torque. Two rotors (Case 1 and Case 2) were made for experiments, one with skew (Case 1) and the other without skew (Case 2). The windings can be seen in Fig. 18. The specifications and design details for the prototype machines are given in Table V.

The back-EMFs of Case 1 (skew) are compared for the results of the developed EMCM, FEA and experiment, as shown in Fig. 19(a), where the skewed waveforms of EMCM are calculated by shifting that of Case 2. The comparison for Case 2 (no skew) is given in Fig. 19(b).

TABLE IV
COMPARISON OF FLUX DENSITY

		Maximum flux density on teeth (T)	Torque (kN.m)
Open Circuit	g=1.5 mm, EMCM	1.19	-
	g=1.5 mm, FEA	1.25	-
	g=3 mm, EMCM	1.20	-
	g=3 mm, FEA	1.20	
Loaded	g=1.5 mm, EMCM	1.70	-
	g=1.5 mm, FEA	1.74	9.28
	g=3 mm, EMCM	1.77	-
	g=3 mm, FEA	1.80	9.20

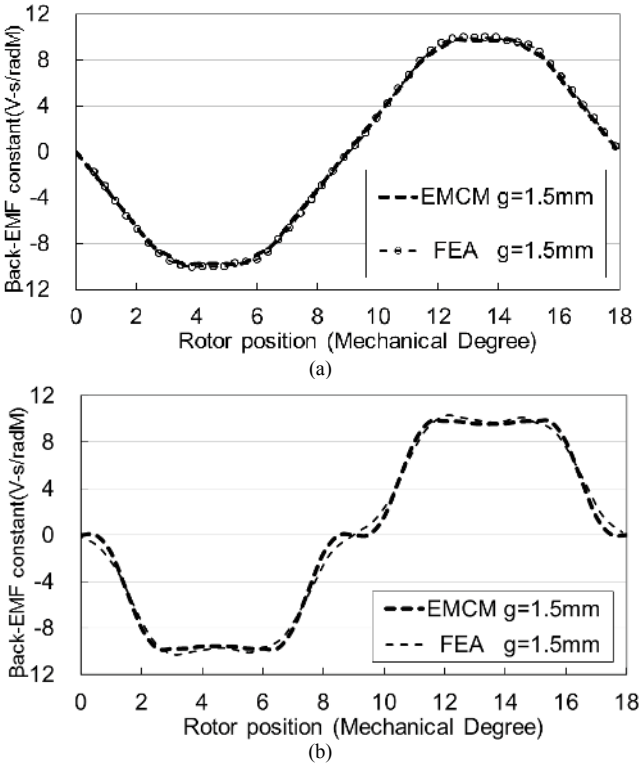

Fig. 14 The comparison of the 540kW machine back-EMF constant: (a) with skew and (b) without skew.

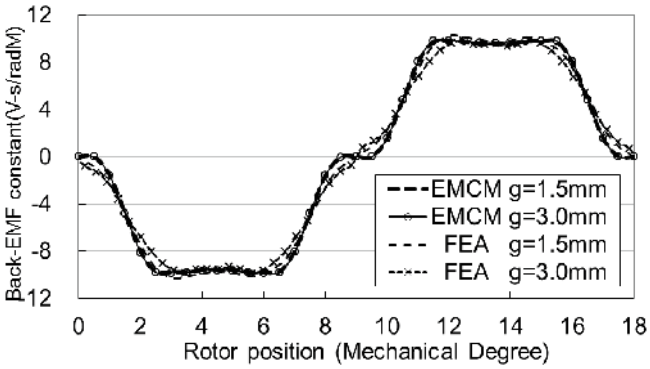

Fig. 15 The comparison of the 540kW machine back-EMF constants between FEA and proposed model for original and large air gap designs (without skew).

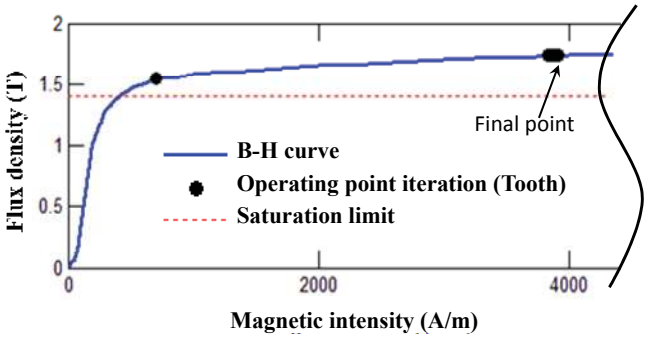

Fig. 16 Calculation process for operating point of tooth material when machine loaded. The figure was generated using a computer program. The saturation limit is user-defined.

(a) (b)

Fig. 17 Features of the rotors (magnets included): (a) with 3.75°M skew (Case 1); (b) without skew (Case 2). The skew for (a) is a step skew which uses two axial rotor sections with an angular offset.

Fig. 18 The stator windings

TABLE V
DESIGN RESULTS OF 350 W PROTOTYPE

Machine Parameters				
Slot number		24	Stack length (mm)	45
Pole number		16	Rotor radius (mm)	29.7
Slot-fill factor (%)		39.5	Generator outer radius (mm)	44.17
Air-gap length (mm)		0.5	Magnet length (mm)	2.3
Tooth width (mm)		5	Gap between magnets (°M)	2.25
Phase back EMF constant (V*sec/radM)		0.4	Series coils per phase	1
			Slot area (mm^2)	51.2
Rated current (dc) after rectifier (A)		2.75	Slot depth (mm)	11.63
Rated speed (r.p.m.)		2000	Bare copper wire dia. (mm)	0.75
Magnet (N35H)	B_r (T)	1.17-1.21	Number of turns per coil	20
	H_c (kA/m)	830-907	Slot opening (mm)	2

The harmonics of the back EMF in Case 2 are analyzed, as shown in Fig. 20. The EMCM approach can successfully calculate the 5th harmonic but the 7th and 13th harmonics are additionally generated due to the fact that the magnet poles are arranged to fit the slots in the EMCM. Since the magnitude of the 5th harmonic is larger than that of the 7th and 13th, the additional harmonics do not significantly affect the main waveforms.

To verify the design, experiments were conducted to load the machine at 500 rpm, 1000 rpm, 1500 rpm and 2000 rpm, respectively. Fig. 21 shows the output power and torque versus output rectified dc current (generator). The machine can achieve rated 350 W output at 2000 rpm, and the torque versus current is linear with similar slopes for all the cases. The FEA gives slightly higher output power which may be due to the exclusion of mechanical and iron losses. Nevertheless, this again confirms the proposed EMCM.

IV. CONCLUSIONS

An equivalent magnetic circuit model has been proposed for the design and analysis of PM electric machines with any pole-slot combinations. A permanent-magnet model has been constructed as a function of slot numbers. Subsequently, a circular model was developed to include all the poles and slots for improving the accuracy. An iterating technique to obtain accurate permeability affected by external sources was also developed to work with the model. The accuracy of the proposed model has been verified by FEA on a 540 kW machines with various scenarios (different air gaps, with rated load or unloaded), and by both FEA and experiments on a 350 W 16-pole 24-slot prototype. The capability of obtaining the entire machine flux patterns by simultaneously taking all the winding MMFs into account has been demonstrated. The developed model is sufficiently accurate for the design of PM machines without the aid of time-consuming finite element analysis.

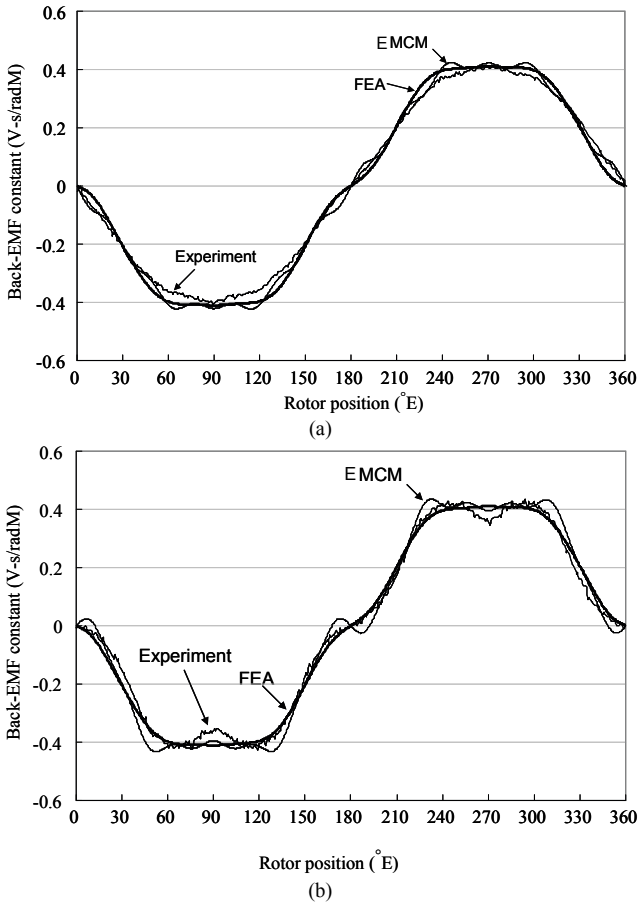

Fig. 19 Comparison of Back-EMF constant waveforms: (a) Case 1 (skew) and (b) Case 2 (without skew)

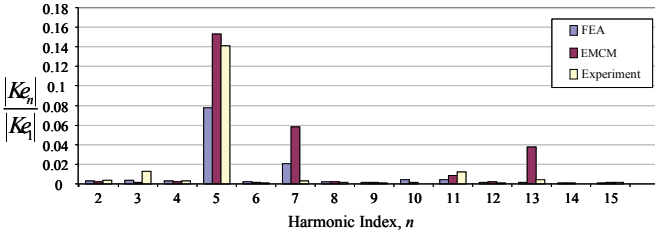

Fig. 20 Harmonic analyses of Back-EMF constant waveform where Ke_1 represents the first harmonic of the waveform.

ACKNOWLEDGEMENTS

The authors are grateful for the computer time and facilities provided by the National Center for High-Performance Computing. The authors would also like to thank Yu-Han Yeh and Wan-Yu Wu for their kind assistance during the research period.

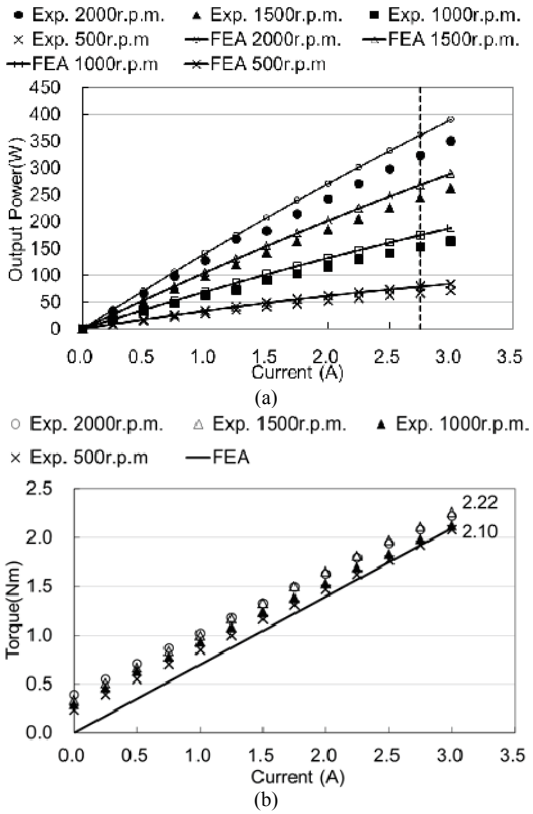

Fig. 21 FEA and experimental results: (a) power vs current; (b) torque vs current. The dashed line in (a) indicates the designed current, at which the experimental output is slightly lower than rated 350 W.

APPENDIX

The sub-matrice in matrix G are given in the following (A.1-A.21).

$$G_1=\begin{bmatrix}\frac{1}{R_{s1}} & 0 & \cdots & 0\\ 0 & \frac{1}{R_{s2}} & & \vdots\\ \vdots & & \ddots & 0\\ 0 & \cdots & 0 & \frac{1}{R_{sN_s}}\end{bmatrix}_{N_s\times N_s} \tag{A.1}$$

$$G_2=\begin{bmatrix}\frac{-1}{R_{s1}} & 0 & \cdots & 0\\ 0 & \frac{-1}{R_{s2}} & & \vdots\\ \vdots & & \ddots & 0\\ & & & \frac{-1}{R_{sN_s}}\\ 0 & \cdots & 0 & 0\end{bmatrix}_{N_s\times(N_s-1)} \tag{A.2}$$

$$G_3=G_4=G_5=[0]_{N_s\times N_s} \tag{A.3}$$

$$G_6=G_2^T \tag{A.4}$$

$$G_7=\begin{bmatrix}\frac{1}{R_{s1}}+\frac{1}{R_{t2}} & 0 & \cdots & 0\\ 0 & \frac{1}{R_{s2}}+\frac{1}{R_{t3}} & & \vdots\\ \vdots & & \ddots & 0\\ 0 & \cdots & 0 & \frac{1}{R_{s(N_s-1)}}+\frac{1}{R_{tN_s}}\end{bmatrix}_{(N_s-1)\times(N_s-1)} \tag{A.5}$$

$$G_8=\begin{bmatrix}0 & \frac{-1}{R_{t2}} & 0 & \cdots & 0\\ 0 & 0 & \frac{-1}{R_{t3}} & & \vdots\\ \vdots & & & \ddots & 0\\ 0 & \cdots & & 0 & \frac{-1}{R_{tN_s}}\end{bmatrix}_{(N_s-1)\times N_s} \tag{A.6}$$

$$G_9=G_{10}=[0]_{(N_s-1)\times N_s} \tag{A.7}$$

$$G_{11}=[0]_{N_s\times N_s} \tag{A.8}$$

$$G_{12}=G_8^T \tag{A.9}$$

$$G_{14}=\begin{bmatrix}\frac{-1}{R_{g1}} & 0 & \cdots & 0\\ 0 & \frac{-1}{R_{g2}} & & \vdots\\ \vdots & & \ddots & 0\\ 0 & \cdots & 0 & \frac{-1}{R_{gN_s}}\end{bmatrix}_{N_s\times N_s} \tag{A.10}$$

$$G_{15}=G_{16}=[0]_{N_s\times N_s} \tag{A.11}$$

$$G_{17}=G_9^T \tag{A.12}$$

$$G_{18}=G_{14} \tag{A.13}$$

$$G_{20}=\begin{bmatrix}\frac{-1}{R_{m1}} & 0 & \cdots & 0\\ 0 & \frac{-1}{R_{m2}} & & \vdots\\ \vdots & & \ddots & 0\\ 0 & \cdots & 0 & \frac{-1}{R_{mN_s}}\end{bmatrix}_{N_s\times N_s} \tag{A.14}$$

$$G_{21}=[0]_{N_s\times N_s} \tag{A.15}$$

$$G_{22}=[0]_{N_s\times(N_s-1)} \tag{A.16}$$

$$G_{23} = G_{21} \tag{A.17}$$

$$G_{24} = G_{20} \tag{A.18}$$

$$G_{13} = \begin{bmatrix} \frac{2}{R_l}+\frac{1}{R_{t1}}+\frac{1}{R_{g1}} & \frac{-1}{R_l} & 0 & \cdots & 0 & \frac{-1}{R_l} \\ \frac{-1}{R_l} & \frac{2}{R_l}+\frac{1}{R_{t2}}+\frac{1}{R_{g2}} & \frac{-1}{R_l} & & & 0 \\ 0 & \frac{-1}{R_l} & \ddots & \ddots & & \vdots \\ \vdots & & \ddots & & \frac{-1}{R_l} & 0 \\ 0 & & & \frac{-1}{R_l} & \frac{2}{R_l}+\frac{1}{R_{t(N_s-1)}}+\frac{1}{R_{g(N_s-1)}} & \frac{-1}{R_l} \\ \frac{-1}{R_l} & 0 & \cdots & 0 & \frac{-1}{R_r} & \frac{2}{R_l}+\frac{1}{R_{tN_s}}+\frac{1}{R_{gN_s}} \end{bmatrix}_{N_s \times N_s} \tag{A.19}$$

$$G_{19} = \begin{bmatrix} \frac{1}{R_{m1}}+\frac{1}{R_{g1}} & 0 & 0 & \cdots & 0 & 0 \\ 0 & \frac{1}{R_{m2}}+\frac{1}{R_{g2}} & 0 & & & 0 \\ 0 & 0 & \ddots & & & \vdots \\ \vdots & & & \ddots & 0 & 0 \\ 0 & & & 0 & \frac{1}{R_{m(N_s-1)}}+\frac{1}{R_{g(N_s-1)}} & 0 \\ 0 & 0 & \cdots & 0 & 0 & \frac{1}{R_{mN_s}}+\frac{1}{R_{gN_s}} \end{bmatrix}_{N_s \times N_s} \tag{A.20}$$

$$G_{25} = \begin{bmatrix} \frac{1}{R_{m1}}+\frac{1}{R_{r5}}+\frac{1}{R_{r1}} & \frac{-1}{R_{r1}} & 0 & \cdots & 0 & \frac{-1}{R_{rN_s}} \\ \frac{-1}{R_{r1}} & \frac{1}{R_{m2}}+\frac{1}{R_{r1}}+\frac{1}{R_{r2}} & \frac{-1}{R_{r2}} & & & 0 \\ 0 & \frac{-1}{R_{r2}} & \ddots & \ddots & & \vdots \\ \vdots & & \ddots & & \frac{-1}{R_{r(N_s-2)}} & 0 \\ 0 & & & \frac{-1}{R_{r(N_s-2)}} & \frac{2}{R_r}+\frac{1}{R_g} & \frac{-1}{R_{r(N_s-1)}} \\ \frac{-1}{R_{rN_s}} & 0 & \cdots & 0 & \frac{-1}{R_{r(N_s-1)}} & \frac{1}{R_{mN_s}}+\frac{1}{R_{g(N_s-1)}}+\frac{1}{R_{gN_s}} \end{bmatrix}_{N_s \times N_s} \tag{A.21}$$

REFERENCES

[1] N. P. Shah, A. D. Hirzel and B. Cho, "Transmissionless selectively aligned surface-permanent-magnet BLDC motor in hybrid electric vehicles," *IEEE Transactions on Industrial Electronics*, vol. 57, no. 2, pp. 669-677, Feb. 2010.

[2] K.I. Laskaris and A. G. Kladas, "Internal permanent magnet motor design for electric vehicle drive," *IEEE Transactions on Industrial Electronics*, vol. 57, no. 1, pp. 138-145. Jan. 2010.

[3] K.T. Chau, C.C. Chan and C. Liu, "Overview of permanent-magnet brushless drives for electric and hybrid electric vehicles," *IEEE Transactions on Industrial Electronics*, vol. 55, no. 6, pp. 2246-2257, Jun. 2008.

[4] S. Zhang, K. Tseng, M. Vilathgamuwa and D. Nguyen, "Design of a robust grid interface system for PMSG-based wind turbine generators," *IEEE Transactions on Industrial Electronics*, Digital Object Identifier: 10.1109/TIE.2010.2044737.

[5] A. Parker, C. Ng, and L. Ran, "Fault tolerant control for a modular generator-converter scheme for direct drive wind turbines," *IEEE Transactions on Industrial Electronics*, Digital Object Identifier: 10.1109/TIE.2010.2045318.

[6] A. Di Gerlando, G. Foglia, R. Perini and M. Iacchetti, "Axial flux PM machines with concentrated armature windings: design analysis and test validation of wind energy generators," *IEEE Transactions on Industrial Electronics*, Digital Object Identifier: 10.1109/TIE.2010.2081956.

[7] J. Sopanen, V. Ruuskanen, J. Nerg and J. Pyrhonen, "Dynamic torque analysis of a wind turbine drive train including a direct-driven permanent magnet generator," *IEEE Transactions on Industrial Electronics*, Digital Object Identifier: 10.1109/TIE.2010.2087301.

[8] S. Ben Elghali, M. Benbouzid, J. Charpentier, T. Ahmed-Ali and I. Munteanu, "Experimental validation of a marine current turbine simulator: application to a PMSG-based system second-order sliding mode control," *IEEE Transactions on Industrial Electronics*, Digital Object Identifier: 10.1109/TIE.2010.2050293

[9] K. T. Chau, M. Cheng and C. C. Chan, "Nonlinear magnetic circuit analysis for a novel stator doubly fed doubly salient machine," *IEEE Tranactions on Magnetics*, vol. 38, no. 5, pp. 2382-2384, Sep. 2002.

[10] P. Campbell, "Magnetic circuit of an axial field D.C. electrical machine," *IEEE Tranactions on Magnetics*, vol. 11, no. 5, pp. 1541-1543, Sep. 1975.

[11] J. D. Law, T. J. Busch, and T. A. Lipo, "Magnetic circuit modeling of the field regulated reluctance machine Part I: model development," *IEEE Transactions on Energy Conversion*, vol. 11, no. 1, pp. 56-61, Mar. 1996.

[12] H. Polinder, J. G. Slootweg, M. J. Hoeijmakers and J. C. Compter, "Modeling of a linear PM machine including magnetic saturation and end effects: Maximum force-to-current ratio," *IEEE Transactions on Industry Applications*, vol.39, no. 6, pp. 1681-1688, Nov./Dec. 2003.

[13] V. Litovski and M. Zwolinski, *VLSI Circuit Simulation and Optimization,* Kluwer Academic Publishers, 1997.

[14] P. C. Roberts, R. A. McMahon, P. J. Tavner, J. M. Maciejowski and T. J. Flack, "An equivalent circuit for the brushless doubly fed machine (BDFM) including parameter estimation and experimental verification," *IEE Proceedings: Electric Power Applications*, vol. 152(4), pp. 933 – 942, 2005.

[15] D. C. Hanselman, *Brushless Permanent Magnet Motor Design*, 2/E, The Writers' Collective, 2003.

[16] H. C. Roters, *Electromagnetic Devices*, John Wiley & Sons, Inc., NewYork, 1941.

[17] E C. Cherry, "The duality between interlinked electric and magnetic circuits," *Proceedings of the Physical Society* [B], 62, pp. 101, 1949.

[18] E. R. Laithwaite, "Magnetic equivalent circuits for electrical machines," *Proceedings of IEE*, vol. 114(11), pp. 1805-1809, Nov. 1967.

[19] C. J. Carpenter, , "Magnetic equivalent circuits," *Proceedings of IEE*, pp. 1503-1511, Oct. 1968.

[20] B. Nady, "Two-dimensional field analysis of cylindrical machines with permanent magnet excitation," *IEEE Transactions on Industry Applications*, vol. IA-20, no. 5, pp. 1267-1276, Sep./Oct. 1984.

[21] O. Vlado, "A method for evaluation of transient and steady state performance in saturated squirrel cage induction machines," *IEEE Transactions on Energy Conversion*, vol. EC-1, no. 3, pp. 190-196, Sep. 1986.

[22] O. Vlado, "Computation of saturated permanent-magnet motor performance by means of magnetic circuit," *IEEE Transactions on Industry Applications*, vol. 1A-23, no. 5, pp. 836-841, Sep./Oct. 1987.

[23] O. Vlado, "A novel method for evaluation of transient states in saturated electric machines," *IEEE Transactions on Industry Applications*, vol. 25, no. 1, pp. 96- 100, Jan./Feb. 1989.

[24] R. S. Gordon, "An equivalent circuit approach to analysis of synchronous machines with saliency and saturation," *IEEE Transactions on Energy Conversion*, vol. 5, no. 3, pp. 538-545, Sep. 1990.

[25] T. J. Busch., J. D. Law. and T. A. Lipo., "Magnetic circuit modeling of the field regulated reluctance machine Part II: saturation modeling and results," *IEEE Transactions on Energy Conversion*, vol. 11, no. 1, pp. 56-61, Mar. 1996.

[26] A. T. Hamid, S. A. Mohammed and G. P. Alexander, "A method for dynamic simulation of air-gap eccentricity in induction machines," *IEEE Transaction on Industry Applications*, vol. 32, no. 4, pp. 910-918, Jul./Aug. 1996.

[27] T. J. E. Miller and J. R. Hendershot, *Design of Brushless Permanent-Magnet motors*, Magna Physics Publishing and Clarendon Press Oxford, 1994.

[28] M. Cheng, K. T. Chau, C. C. Chan, E. Zhou and X. Huang, "Nonlinear varying-network magnetic circuit analysis for doubly salient permanent-magnet motors," *IEEE Transactions on magnetics*, vol. 36, no. 1, pp.339-348, Jan. 2000.

[29] Y. Kano, K. Tonogi, T. Kosaka and N. Matsui, "Torque-maximizing design of double-stator axial-flux, PM machines using simple non-linear magnetic analysis," *IEEE Industry Applications Conference*, pp.875-881, Oct. 2007.

[30] Y. Chen, Z. Q. Zhu and D. Howe, "Three-dimensional lumped-parameter magnetic circuit analysis of single-phase flux-switching permanent-magnet motor," *IEEE Transactions on Industry Applications*, vol. 44, no. 6, pp. 1701-1710, Nov./Dec. 2008.

[31] S.H. Han, T.M. Jahns and W.L. Soong,"A magnetic circuit model for an IPM synchronous machine incorporating moving airgap and cross-coupled saturation effects," *IEEE International Electric Machines and Drives Conference*, Antalya, Turkey, May 3-5, 2007.

[32] Characteristic Curves of Magnetic Properties of Magnetic Steel Core. Kaohsiung, Taiwan: China Steel Corp., 2004.

[33] F.W. Carter, "The magnetic field of the dynamic-electric machine," *Journal IEE*, vol.64, pp.1115, 1926.

Min-Fu Hsieh (M'02) was born in Tainan, Taiwan in 1968. He received the BEng degree in mechanical engineering from National Cheng Kung University (NCKU), Tainan, Taiwan in 1991. He then received the MSc and PhD degrees in mechanical engineering from the University of Liverpool, UK in 1996 and 2000, respectively. From 2000 to 2003, he served as a researcher in the Electric Motor Technology Research Center at NCKU. In 2003, he joined the Department of Systems and Naval Mechatronic Engineering, NCKU as an assistant professor. His area of interests includes renewable energy generation (wave, tidal current and wind), electric propulsors, servo control, and electric machine design. In 2007, he was promoted to associate professor. Dr. Hsieh is a member of the IEEE Magnetics, Industrial Electronics, Oceanic Engineering, and Industrial Applications Societies.

You-Chiuan Hsu received his BEng and MEng degrees from the Department of Systems and Naval Mechatronic Engineering of National Cheng Kung University, Tainan, Taiwan in 2004 and 2006, respectively. He is currently working toward the PhD degree in the same department. In 2009, he spent eight months in the Department of Engineering of University of Cambridge, UK, as an official visitor. His current research interests include wind generator system, permanent magnet generator/motor design, power electronics, electric machine driver design and post-assembly magnetization method. He has over 15 publications.